

Universal sublinear resistivity in vanadium kagome materials hosting charge density waves

Shirin Mozaffari ^{1,*}, William R. Meier ¹, Richa P. Madhogia¹, Nikolai Peshcherenko,² Seoung-Hun Kang,³ John W. Villanova ⁴, Hasitha W. Suriya Arachchige,⁵ Guoxin Zheng,⁶ Yuan Zhu ⁶, Kuan-Wen Chen ⁶, Kaila Jenkins ⁶, Dechen Zhang,⁶ Aaron Chan,⁶ Lu Li,⁶ Mina Yoon,⁴ Yang Zhang,^{5,7} and David G. Mandrus^{1,3,5,†}

¹*Department of Materials Sciences and Engineering, University of Tennessee, Knoxville, Tennessee 37996, USA*

²*Max Planck Institute for Chemical Physics of Solids, 01187 Dresden, Germany*

³*Materials Science and Technology Division, Oak Ridge National Laboratory, Oak Ridge, Tennessee 37831, USA*

⁴*Center for Nanophase Materials Sciences, Oak Ridge National Laboratory, Oak Ridge, Tennessee 37831, USA*

⁵*Department of Physics and Astronomy, University of Tennessee, Knoxville, Tennessee 37996, USA*

⁶*Department of Physics, University of Michigan, Ann Arbor, Michigan 48109, USA*

⁷*Min H. Kao Department of Electrical Engineering and Computer Science, University of Tennessee, Knoxville, Tennessee 37996, USA*



(Received 25 May 2023; revised 2 May 2024; accepted 24 June 2024; published 12 July 2024)

The recent discovery of a charge density (CDW) state in ScV_6Sn_6 at $T_{\text{CDW}} = 91$ K offers new opportunities to understand the origins of electronic instabilities in topological kagome systems. By comparing to the isostructural non-CDW compound LuV_6Sn_6 , we unravel interesting electrical transport properties in ScV_6Sn_6 , above and below the charge-ordering temperature. We observed that by applying a magnetic field along the a axis, the temperature behavior of the longitudinal resistivity in ScV_6Sn_6 changes from metal-like to insulator-like above the CDW transition. We show that in the charge-ordered state ScV_6Sn_6 follows the Fermi liquid behavior while above that, the resistivity varies sublinearly over a broad temperature range. The sublinear resistivity, which scales by $T^{3/5}$ is a common feature among other vanadium-containing kagome compounds exhibiting CDW states such as KV_3Sb_5 , RbV_3Sb_5 , and CsV_3Sb_5 . By contrast, the sublinear behavior of the resistivity does not occur in LuV_6Sn_6 . Finally, we show anomalous Hall-like behavior in ScV_6Sn_6 below T_{CDW} , which is absent in the Lu compound. Comparing the transport properties of ScV_6Sn_6 and LuV_6Sn_6 is valuable to highlight the impacts of the unusual CDW in the Sc compound.

DOI: [10.1103/PhysRevB.110.035135](https://doi.org/10.1103/PhysRevB.110.035135)

I. INTRODUCTION

Kagome lattices comprised of appropriate constituents have the potential to host magnetism and novel topological electronic phenomena [1]. The connectivity of this lattice gives a characteristic electronic structure with Dirac points, flat bands, and van Hove singularities (VHS) [2]. Tuning the Fermi level into one of these interesting features in the band structure can induce electronic instabilities such as charge density waves (CDW), chiral spin density waves, superconductivity, and non-Fermi liquid behavior [3–5].

The hexagonal 135 families of compounds (AV_3Sb_5 with $A = \text{K, Rb, Cs}$) host curious CDWs with a 2×2 in-plane ordering, and unconventional superconductivity tied to their vanadium kagome sheets [6–11]. Additionally, the normal states of the 135 families are identified as \mathbb{Z}_2 topological metals with band inversion [6,10], the CDW state shows a pair density wave [12], nematic order [13], and a large anomalous Hall response [14,15] in the absence of resolvable magnetic order [16]. Thus, there is a notable concurrence of intriguing phenomena owing to the vanadium kagome lattice.

The newly discovered vanadium kagome metal, ScV_6Sn_6 , also hosts a CDW below $T = 92$ K and shares the stacked vanadium kagome sheets critical to the unique behavior in the 135 family [17]. ScV_6Sn_6 belongs to a large family of intermetallics RT_6X_6 , ($R = \text{rare earth}; T = \text{V, Cr, Mn, Fe, Co}; X = \text{Ge, Sn}$). Magnetism and nontrivial topological electronic properties are common features among this family [18–26]. In contrast to the 135 family, the V atoms in ScV_6Sn_6 form kagome bilayers, and the CDW is associated with a $\sqrt{3} \times \sqrt{3}$ in-plane ordering, and a tripling of the unit cell along the c axis [17]. Curiously, the isoelectronic LuV_6Sn_6 and YV_6Sn_6 do not develop the CDW observed in ScV_6Sn_6 [24,27].

The CDW in ScV_6Sn_6 has some unique characteristics. There are strong CDW fluctuations above the CDW transition with a different period than the low-temperature ordered phase [28] demonstrating competing CDW modes [29]. The magnetic susceptibility [17] and optical conductivity [30] reveal a drop in the number of carriers on cooling through T_{CDW} . Despite this, resistivity drops through the transition due to a decreased electronic scattering by CDW fluctuations [30]. Although the Fermi level is dominated by d orbitals from the vanadium kagome nets, the charge density wave has little impact on V positions [17] or their bands [31–34]. In fact, the most prominent CDW gap appears in a band associated with Sn orbitals [35], highlighting the involvement of Sn in the CDW [27]. Finally, Ref. [36] argues that the CDW

*Contact author: smozaff1@utk.edu

†Contact author: dmandrus@utk.edu

in ScV_6Sn_6 breaks time-reversal symmetry based on muon spin rotation measurements. Most of the enticing phenomena observed in the kagome compounds are linked to the proximity of their VHSs to the Fermi level; common features in the electronic structure, which drive correlations. A universal long-range Coulomb behavior [37] is also reported as a hallmark of kagome metals. Our observation of sublinear resistivity behavior in the 135 and 166 kagome metals adds another intriguing phenomenon to the list of peculiar properties in this family of compounds.

We undertake a detailed study on electrical transport and magnetic properties of ScV_6Sn_6 and its sister compound LuV_6Sn_6 . Although their electronic structures are nearly identical, our results suggest the Lu compound does not host a CDW. We compare these isostructural compounds to explore how unusual CDW order and fluctuation impact the transport properties ScV_6Sn_6 uncovering three key observations. First, both above and below the transition temperature ScV_6Sn_6 have a remarkably large magnetoresistance for current along the c axis. Second, we observe a $T^{3/5}$ dependence of the resistivity on the temperature in ScV_6Sn_6 above T_{CDW} , which is absent in CDW-free LuV_6Sn_6 . The scaling of resistivity by $T^{3/5}$ is also observed in KV_3Sb_5 , RbV_3Sb_5 , and CsV_3Sb_5 suggesting this sublinear resistivity is a universal phenomenon in the vanadium CDW kagome metals above T_{CDW} . Third, we note that ScV_6Sn_6 exhibits anomalous Hall effect-like behavior below T_{CDW} that is absent in the Lu compound. Our study establishes comparisons of ScV_6Sn_6 and LuV_6Sn_6 as a critical tool in future understandings of the nature of the CDW in ScV_6Sn_6 .

II. EXPERIMENTAL DETAILS

Growth and characterization. ScV_6Sn_6 and LuV_6Sn_6 were synthesized via the tin flux method with a starting atomic ratio of $\text{Sc/Lu:V:Sn} = 1:6:60$. Sc/Lu pieces (Alfa Aesar 99.9%), V pieces (Alfa Aesar 99.8%), and Sn shot (Alfa Aesar 99.9999%) were loaded into an alumina Canfield crucible set. The crucible assembly was sealed within a fused silica ampule, heated to 1150 °C over 12 h, held for 15 h, and cooled to 780 °C over 300 h. At this temperature, the flux was separated from the crystals by inverting the tube and centrifuging. This procedure yielded bulky, hexagonal metallic crystals with typical lateral dimensions of 0.5–4 mm in size. The elemental composition and approximate stoichiometry of the structure were confirmed via scanning electron microscopy (SEM)/energy-dispersive spectroscopy (EDS). A powder x-ray diffraction (XRD) measurement was performed using a Bruker D2 Phaser equipped with a $\text{Cu } K_\alpha$ x-ray source. Figures S1 and S2 within the Supplemental Material (SM)[38] confirm the $P6/mmm$ HfFe_6Ge_6 -type structure for both samples. Conventional magnetotransport experiments were performed in a physical property measurement system (Quantum Design-PPMS) under magnetic fields up to $\mu_0 H = 9$ T and temperatures as low as 1.8 K. The resistivity was measured with the standard four-probe method with the electrical current applied in the ab plane and out-of-plane. Magnetization measurements were performed in a commercial superconducting quantum interference device

magnetometer (Quantum Design). We define $\mathbf{x} \parallel \mathbf{a}$, $\mathbf{y} \parallel \mathbf{c} \times \mathbf{a}$, and $\mathbf{z} \parallel \mathbf{c}$, which is depicted by the cartoon in Fig. 4 below.

Simulations. We performed *ab initio* calculations based on density functional theory (DFT) [39,40] as implemented in the Vienna *ab initio* simulation package (VASP) [41] with projector augmented wave potentials [42] and spin-orbit coupling. The Perdew-Burke-Ernzerhof (PBE) form [43] was employed for the exchange-correlation functional with the generalized gradient approximation (GGA). The energy cutoff was set to 520 eV for all calculations. The Brillouin zone was sampled using a $31 \times 31 \times 31$ Γ -centered k grid. Atomic relaxations were done until the Hellmann-Feynman force acting on every atom became smaller than 0.01 eV/Å. We calculate the density of states (DOS) using a tight binding model constructed from an automatic Wannierization scheme [44] with FPLO [45]. The momentum space integration mesh is $100 \times 100 \times 100$ to account for the fine variations around the Fermi level, which can be important for comparison with the experimentally measured magnetic susceptibility and resistivity.

III. RESULTS AND DISCUSSION

A. Band structures

The compounds ScV_6Sn_6 and LuV_6Sn_6 share numerous features, as demonstrated by their extremely similar orbital-projected electronic band structures. Specifically, both compounds exhibit a kagome lattice that displays a Dirac point at the K point situated below the Fermi level (E_F), a saddle point near E_F and a flat band positioned above E_F level by 0.3 eV throughout the entire Brillouin zone in the $k_z = 0$ plane. These compounds have a few Dirac points, the one close to E_F and other interesting features are marked in Fig. 1(b).

Notably, the band characterized by the d_{z^2} orbital component is noncontinuous along the M–K line due to interactions with nonorthogonal d_{xz} and d_{yz} orbital bands. Upon closer inspection, however, ScV_6Sn_6 exhibits smaller-sized electron pockets near the M points highlighted by the blue shaded region in Figs. 1(b) and 1(d) relative to LuV_6Sn_6 . These diminutive pockets may facilitate superior carrier mobility, which enhances electrical conductivity. The Fermi surface of ScV_6Sn_6 displays a higher Fermi velocity than LuV_6Sn_6 nearly everywhere throughout the Brillouin zone, especially near $k_z = 0.5$ by a factor of 1.5 [Figs. 1(c) and 1(e)], which enhances the carrier mobility. Besides the nearly flat band around 300 meV above E_F , there also exists significant van Hove singularities at the hole side in ScV_6Sn_6 . The band structure of ScV_6Sn_6 below the CDW phase is presented in Refs. [33,46]. We present the calculated DOS in Fig. S5 within the SM [38]. We found that in ScV_6Sn_6 the VHS peak is very close to the Fermi level, $E_{\text{VHS}} = -80$ meV for $T > T_{\text{CDW}}$. In the CDW state, the VHS moves away to $E_{\text{VHS}} = -165$ meV. This departure of the VHS away from E_F leads to modification of the magnetic susceptibility and resistivity, which we explain in Secs. III B and III C.

B. Magnetic susceptibility and electrical resistivity

Sc and Lu are both nonmagnetic trivalent rare-earth elements, so we expect strong chemical and physical similarities.

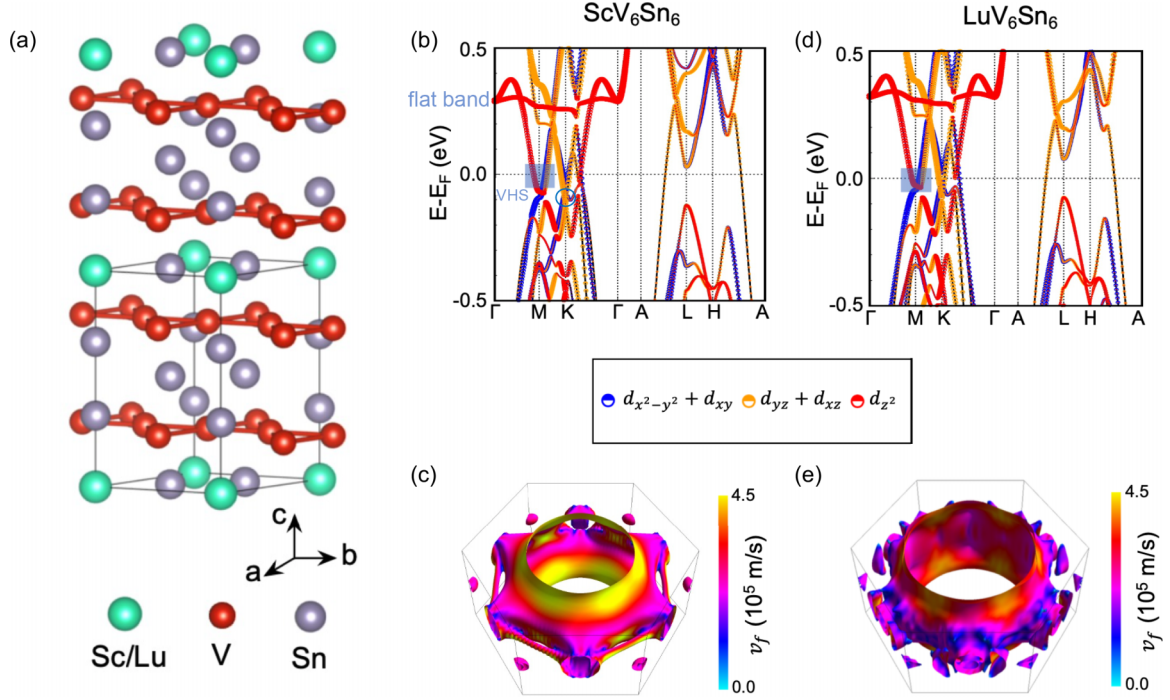


FIG. 1. Crystal and electronic structures of kagome metals ScV_6Sn_6 and LuV_6Sn_6 . (a) Crystal structure of $RV_6\text{Sn}_6$, $R = \text{Sc}$ and Lu . (b) Orbital-projected band structure with the V - d orbitals for ScV_6Sn_6 and (d) for LuV_6Sn_6 . The blue circle in panel (b) indicates the position of the Dirac point. The blue shaded area in (b) and (d) shows the size of the electron pockets near the M points. [(c),(e)] The Fermi surface of ScV_6Sn_6 and LuV_6Sn_6 , respectively, are colored according to the Fermi velocity of the bands.

Although the ionic radius of Lu^{3+} is about 12.3% larger than Sc^{3+} [47], this only produces a subtle 1% increase in unit-cell volume. The refined structural parameters from our XRD measurements, which are listed in Table I, are consistent with our DFT result and those in previous studies [48]. The similar chemistry of Sc and Lu is also revealed by their nearly identical electronic structures (Fig. 1). Both ScV_6Sn_6 and LuV_6Sn_6 adopt the $P6/mmm$ space group, with the unit cell containing two kagome layers composed of vanadium atoms. These layers are enclosed by Sn and ScSn/LuSn layers along the out-of-plane direction in ScV_6Sn_6 and LuV_6Sn_6 , respectively. As shown in Table I, the DFT lattice parameters of ScV_6Sn_6 are found to be $a = 5.45403 \text{ \AA}$ and $c = 9.23111 \text{ \AA}$, while those of LuV_6Sn_6 are $a = 5.50286 \text{ \AA}$ and $c = 9.22634 \text{ \AA}$. These values are in agreement with experimental measurements, which show that the a lattice parameter of ScV_6Sn_6 is smaller than that of LuV_6Sn_6 , and the c lattice parameter of the former is larger than that of the latter. Figure 2(a) presents the magnetic susceptibility χ as a func-

TABLE I. Lattice parameters and R^{3+} ionic radius [47] for $RV_6\text{Sn}_6$, $R = (\text{Sc}, \text{Lu})$, and charge-ordering temperature. The experimental lattice parameters are obtained from the Rietveld refinement and DFT in this study.

	Ionic radius (\AA)	a (\AA)	c (\AA)	$T_{\text{CDW}}(K)$
ScV_6Sn_6	0.870	5.47488(6)	9.1764(1)	91
DFT		5.45304	9.23111	
LuV_6Sn_6	0.977	5.50286(5)	9.1738(1)	no CDW
DFT		5.48307	9.22634	

tion of temperature T for the Sc and Lu compounds. Note that the magnitude has similar small values [about $1 \times 10^{-3} \text{ emu} (\text{mol } RV_6\text{Sn}_6)^{-1} \text{ Oe}^{-1}$ or $7.7 \times 10^{-5} \text{ cm}^3 (\text{mol atoms})^{-1}$] consistent with weak Pauli paramagnetism from metals without strongly magnetic atoms [49]. Importantly, $\chi(T)$ of ScV_6Sn_6 drops at $T_{\text{CDW}} = 91 \text{ K}$ consistent with the CDW observed previously [17]. This is absent in the Lu material, suggesting it does not develop a CDW. Finally, note that the Lu material has a near temperature independent $\chi(T)$, in agreement with Ref. [24], while ScV_6Sn_6 has a decreasing $\chi(T)$ on cooling from room temperature to $T = T_{\text{CDW}}$. The electronic contribution to the magnetic susceptibility reflects the DOS near the Fermi level with thermal broadening [50],

$$\chi(T) = \mu_B^2 \mu_m \int dE D(E) \left(-\frac{df_0(E)}{dE} \right), \quad (1)$$

where μ_B is the Bohr magneton, μ_m is the permeability, $D(E)$ is the DOS, $f_0(E) = [e^{E/(k_B T)} + 1]^{-1}$ is the Fermi-Dirac distribution function, and k_B is the Boltzmann constant. The $\frac{df_0(E)}{dE}$ term produces susceptibility contributions from DOS features near the Fermi level at elevated temperatures [51]. Therefore, we attribute the decrease in $\chi(T)$ for ScV_6Sn_6 during cooling for temperatures above T_{CDW} to the loss of thermally excited carriers from the van Hove feature just below E_F .

Figures 2(b) and 2(c) show the in-plane longitudinal resistivity ρ_{xx} and out-of-plane longitudinal resistivity ρ_{zz} under the application of magnetic field for ScV_6Sn_6 and LuV_6Sn_6 samples. In all the measurements, the magnetic field $\mu_0 H$ was applied perpendicular to the current as depicted by the schematic in Fig. 2(c). Both samples exhibit strong resistive

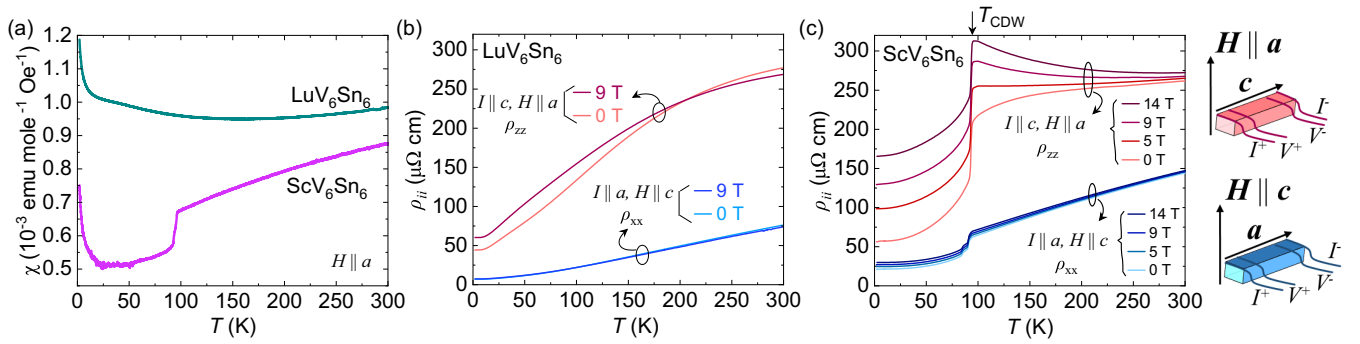


FIG. 2. Magnetotransport properties of $RV_6\text{Sn}_6$. (a) Temperature dependence of magnetic susceptibility χ for ScV_6Sn_6 and LuV_6Sn_6 with the magnetic field H pointing in the plane. Electrical resistivity (ρ) of (b) LuV_6Sn_6 and (c) ScV_6Sn_6 as a function of temperature T under the application of the magnetic field. The resistivity was measured along the a axis (ρ_{xx}) and c axis (ρ_{zz}) of the crystals. Schematics adjacent to panel (c) show the geometry of the measurements. T_{CDW} shows the temperature of the onset of charge ordering. Metal-like to insulator-like behavior through the application of high field is seen above the CDW state in the Sc compound.

anisotropy expected for layered structures with $\rho_{zz} > \rho_{xx}$. This is also consistent with the Fermi velocities in-plane and out-of-plane (Fig. 1). In Fig. 2(c), the CDW transition in ScV_6Sn_6 is clearly evident as a sharp drop in the resistance on cooling for both current directions (ρ_{xx} drops 48.5% and ρ_{zz} drops 43.3%). Note that the CDW transition in ρ_{xx} shows a double transition (seen by others [30,34]). The onset of the first transition, which happens at $T \sim 94$ K, coincides with the single CDW transition in ρ_{zz} . The midpoint of the first transition happens at $T_{\text{CDW}} = 91$ K. The onset of the second step in ρ_{xx} happens at $T \sim 89$ K. We currently do not have a clear explanation for the origin of the second transition, but it might signal a lock-in transition from an incommensurate to a commensurate CDW [52–54]. There is evidence that a phonon mode with a different period is active above T_{CDW} [28,55]. The dramatic drops in resistance are absent in LuV_6Sn_6 again, suggesting it does not develop charge order. Our resistivity measurement for the Lu compound is consistent with that reported in Ref. [24].

We now turn to the evolution of the resistivity under differing magnetic field strengths in these two compounds. The CDW transition temperature in ScV_6Sn_6 is insensitive to magnetic fields up to 14 T. In both compounds, the applied magnetic field has a stronger effect on ρ_{zz} than ρ_{xx} , but the behavior in ScV_6Sn_6 is remarkable. Note that ρ_{zz} rises dramatically with an increasing field below 200 K. The magnitude of this increase is nearly temperature-independent below T_{CDW} and decreases slowly as the sample is heated above the transition. Curiously, above T_{CDW} the slope of $\rho_{zz}(T)$ changes from positive (metal-like) to negative (insulator-like) as the field is increased through 5 T. Using Arrhenius equation, we estimated an activation energy of about 2 meV for this insulating-like behavior above the CDW transition induced by magnetic field (see Sec. S4 within the SM [38]). This temperature-dependent enhancement of ρ_{zz} above T_{CDW} may originate from strong CDW fluctuations that are recently reported in Ref. [28]. This dramatic magnetoresistance behavior of ρ_{zz} in the Sc compound is clearly absent in LuV_6Sn_6 , revealing the anisotropic impact of CDW order and fluctuations on transport in ScV_6Sn_6 .

C. Universal sublinear resistivity

Now we return to the electrical transport properties, with emphasis on ρ_{xx} . Figure 3 shows the temperature dependence of the longitudinal resistivity ρ_{xx} for the current applied along the a axis of the crystal. Above the charge-ordering temperature ρ_{xx} varies sublinearly with temperature. This sublinear behavior is a common feature in most of the kagome metallic compounds [6–8,51,56].

The resistivity versus temperature curves for common metallic materials generally have positive concavity. Temperature dependence of a metallic resistance at zero fields can be modeled by a combination of the power law temperature dependencies $\sum_i \alpha_i T^{\gamma_i}$, where different terms describe different T -dependence scattering phenomena [57]. At high temperatures, the scattering is dominated by phonons, and resistivity grows linearly until the temperature approaches the Debye temperature T_D [58].

Our estimate for the Debye temperature from the heat capacity result reported for ScV_6Sn_6 [17] is $T_D = 316$ K. Therefore, one would expect a linear trend for $\rho_{xx}(T)$ at an intermediate and high temperature within the context of the present experiment. This is indeed the case for LuV_6Sn_6 in which the CDW transition is absent. However, the $\rho_{xx}(T)$ curve for ScV_6Sn_6 deviates from this linear behavior. We modeled the resistivity data to $\rho \propto T^n$ and found that the power-law formula with $n = 0.62 \approx 3/5$ fits the experimental data extremely well for the temperature range 100–400 K, as demonstrated by the red line in Fig. 3(a). For the non-CDW compound, LuV_6Sn_6 , $n = 0.95 \approx 1$ models the resistivity data very well for the measured temperature range 100–300 K.

We performed a similar analysis ($\rho \propto T^n$) on the resistivity of the 135 vanadium kagome metals and found that $n = 3/5$ also fits the resistivity behavior in this vanadium kagome family. The obtained fitting results are $n = 0.61$ for RbV_3Sb_5 , $n = 0.60$ for CsV_3Sb_5 , and $n = 0.67$ for KV_3Sb_5 . We noticed some variations between samples that are measured in different groups, and so within the uncertainty of the experimental fit, we take $n \approx 3/5$. This shows that resistivity varies by $T^{3/5}$ for vanadium kagome compounds exhibiting CDW. In Fig. 3(b) we show that the exponent $n = 3/5$ describes the

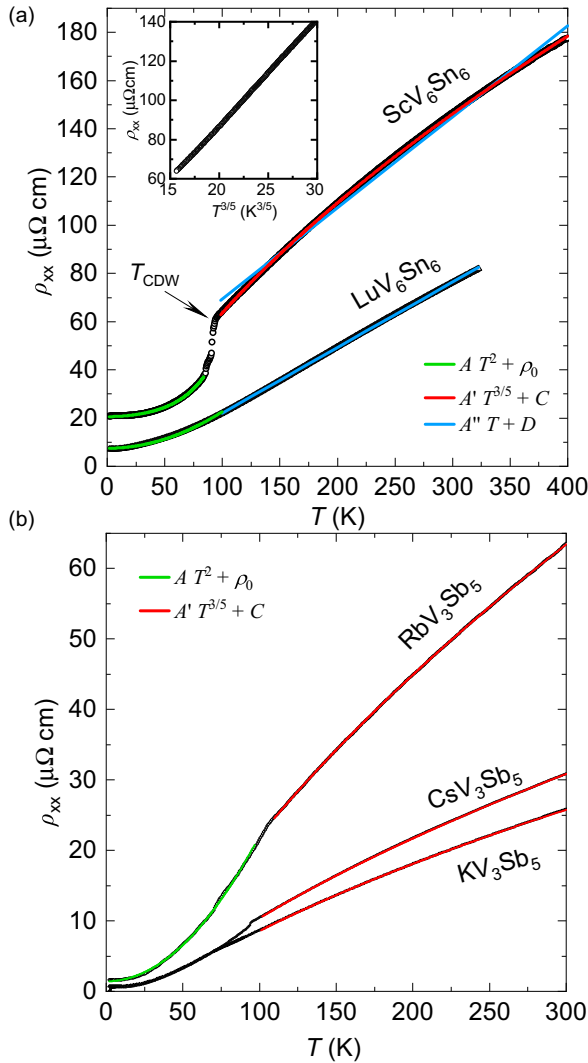


FIG. 3. Resistivity data analysis. Symbols show electrical resistivity of ScV_6Sn_6 and LuV_6Sn_6 in (a) and AV_3Sb_5 ($A = \text{K, Rb, Cs}$) in (b) as a function of temperature, with the electric current applied along the a axis of the crystal. Red- and green-solid lines are fit using equations $\rho = A'T^{3/5} + C$ and $\rho = AT^2 + \rho_0$, respectively. The blue line is a linear fit to the data. $A, A', A'', C, D,$ and ρ_0 are constant. Inset in (a) shows the resistivity above T_{CDW} for ScV_6Sn_6 plotted as the $\rho(T^{3/5})$ dependence, indicating a $T^{3/5}$ behavior at high temperatures. Data for the AV_3Sb_5 materials was digitized from Ref. [59] and the authors of Refs. [6,7].

$\rho(T)$ behavior of KV_3Sb_5 [7], RbV_3Sb_5 [8], and CsV_3Sb_5 [6] samples very well above the charge-ordering temperature.

Analysis of ρ_{xx} displays that below the CDW transition, resistivity follows the T^2 behavior, as shown by the green curves in Figs. 3(a) and 3(b). Similar to ScV_6Sn_6 , the T^2 scaling holds below the CDW transition for the 135 families as well. A T^2 scaling of the resistivity is a signature of the Fermi liquid (FL) behavior in metals. Generally, any deviation from this scaling, such as the linear in T resistivity of high- T_c cuprates [60] and heavy-fermion compounds [61], is loosely defined as non-Fermi liquid (non-FL) behavior [58].

In a separate paper [62], we explore a minimal model that could explain the sublinear resistivity dependence we observe.

D. Hall effect and magnetoresistivity

We have measured the in-plane magnetoresistance MR_{xx} and Hall resistivity ρ_{yx} , and their out-of-plane counterparts, MR_{zz} , and ρ_{yz} , for ScV_6Sn_6 and LuV_6Sn_6 . Magnetoresistance is defined as $\text{MR}_{ii} = [\rho_{ii}(\mu_0 H) - \rho_{ii}(0)] / \rho_{ii}(0) \times 100\%$. In the Hall effect measurements, ρ_{ji} , i indicates the direction in which the electric current was applied, and j indicates the direction of the measured transverse voltage.

Figure 4 presents the magnetoresistance and Hall effect for ScV_6Sn_6 and LuV_6Sn_6 . As pointed out above with Figs. 2(b) and 2(c), magnetoresistance is largest for currents applied along the c axis in both compounds. The MR_{zz} of ScV_6Sn_6 is especially notable, achieving 125% at 9 T and 1.8 K, Fig. 4(c). This reinforces the strong influence of the CDW order on the electronic transport and, therefore, transport properties of the Sc compound.

The general trend of the Hall resistance is nonlinear in both samples, particularly below 150 K. This is consistent with the multi-band nature of these systems (Fig. 1). The dominant Hall responses of ρ_{yx} and ρ_{yz} in LuV_6Sn_6 are qualitatively similar. However, the Hall responses in ScV_6Sn_6 are markedly different among the two measured geometries. In-plane Hall resistance ρ_{yx} in ScV_6Sn_6 [Fig. 4(b)] at $T \leq T_{\text{CDW}}$ shows a negative slope below 1.7 T and a positive slope above that. LuV_6Sn_6 also shows this nonlinear behavior but with the opposite signs. The Hall signal is observed to change sign at higher values of the field. Similar nonlinear behavior has been seen in other compounds of the 166 families, such as YV_6Sn_6 and GdV_6Sn_6 [20,21]. The complex field and temperature evolution of the Hall resistivity suggests the presence of multiple carriers. One may hypothesize that the carrier with a higher (lower) concentration has a lower (higher) mobility and dominates the transport at lower (higher) fields. To estimate the number of number of charge carriers and mobilities, we fitted the in-plane magnetoresistance (MR_{xx}) and Hall resistivity (ρ_{yx}) to the simple two-band model [63,64] through Eq. (S1) within the SM [38]. The two-band model assumes average electron and hole densities and mobilities for electron and hole bands. Note that the two-band model predicts a parabolic behavior for the magnetoresistance as a function of the field, and that is why we obtained better fitting results for the Lu compound. MR_{xx} for ScV_6Sn_6 behaves almost linear with the field at low temperature and thus the fittings are not perfect. Nevertheless, we report the obtained values for n and μ since this model can capture the overall behavior of magnetotransport. The results of simultaneous fittings to Eq. S1, charge carrier densities and mobilities as a function of temperature, are shown in Fig. S3 within the SM [38]. For ScV_6Sn_6 , we obtained electrons that are one order of magnitude less numerous than holes but have almost three times larger mobilities. The dominant type of carrier in LuV_6Sn_6 has an opposite sign and is more numerous compared to ScV_6Sn_6 . The smaller mobility values for the Lu compound compared to the Sc compound agree with the DFT calculation results for the Fermi velocities, shown projected on the Fermi surface [Figs. 1(c) and 1(e)].

The temperature dependence of carriers in ScV_6Sn_6 (Fig. S3 within the SM [38]) shows a clear signature of the CDW transition. There is a drop in hole-like carriers on

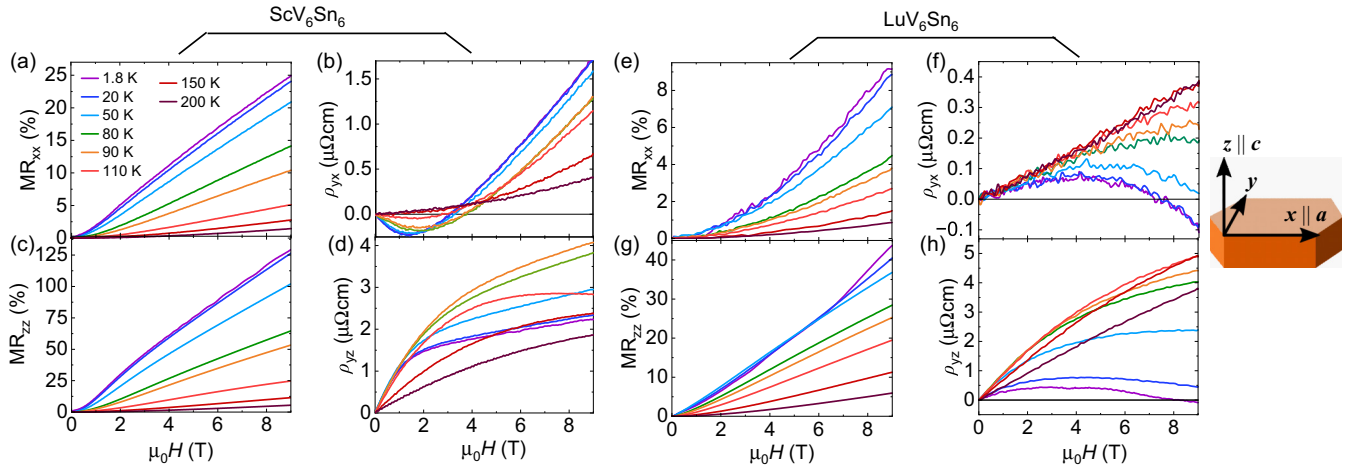


FIG. 4. Comparison of magnetoresistivity (MR_{ii}) and Hall resistivity ρ_{ji} in ScV_6Sn_6 and LuV_6Sn_6 . (a) MR_{xx} and (b) ρ_{yx} as a function of magnetic field μ_0H at various temperatures when $\mu_0H \parallel c$ for ScV_6Sn_6 . (c) Magnetoresistance MR_{zz} and (d) Hall resistivity ρ_{yz} as a function of magnetic field μ_0H at various temperatures when $\mu_0H \parallel a$ for ScV_6Sn_6 . (e) Magnetoresistance MR_{xx} and (f) Hall resistivity ρ_{yx} as a function of magnetic field μ_0H at various temperatures when $\mu_0H \parallel c$ for LuV_6Sn_6 . (g) Magnetoresistance MR_{zz} and (h) Hall resistivity ρ_{yz} as a function of magnetic field μ_0H at various temperatures when $\mu_0H \parallel a$ for LuV_6Sn_6 . The cartoon on the right side, shows the coordinate x , y , and z relative to the crystallographic direction.

cooling through T_{CDW} consistent with the drop in magnetic susceptibility and opening of a CDW gap. The increase in carrier mobility during the formation of the CDW results in the observed drop in resistivity despite the less numerous carriers. Charge carriers in LuV_6Sn_6 also show drastic temperature dependence below 150 K, nonetheless of the fact that no CDW occurs. This is related to the dramatic change of in the slope ρ_{yx} with the magnetic field as we cool the sample.

Anomalous Hall-like behavior

In the 135 materials, the anomalous Hall effect (AHE) has drawn significant attention. A saturating anomalous Hall-like signal is observed in the ab plane, sparking speculation that the CDW breaks time-reversal symmetry [14,15]. Other indications of time-reversal symmetry breaking are the observation of an increase in muon spin relaxation below T_{CDW} [65,66] and magneto-optical Kerr effect [67]. In the case of the latter experiment, there remains debate as an alternative experiment found no discernible Kerr effect [68]. Since long-range magnetic order is absent in the 135 compounds, time-reversal symmetry breaking is explained in terms of loop-current order in the CDW state [3,67]. Do the vanadium kagome metals ScV_6Sn_6 or LuV_6Sn_6 share this AHE behavior?

In Fig. 5, we attempt to capture an AHE in ScV_6Sn_6 and LuV_6Sn_6 . Our emphasis is on the yz direction where the curves for ScV_6Sn_6 below the CDW transition show characteristics of AHE. First, we estimate an ordinary contribution to the Hall signal by fitting the slope of $\rho_{ji}(\mu_0H)$ between 6 and 9 T (inset in Fig. 5). We then subtract to obtain ρ_{ji}^{AHE} to highlight abrupt changes in slope that others have identified as an anomalous Hall contribution.

The procedure yields smooth and kink-free curves for ρ_{yx}^{AHE} for both compounds at $T = 20$ and 100 K. We tie the nonlinear Hall behavior in both compounds to the multi-band Fermi surfaces. Only the ρ_{yz}^{AHE} from ScV_6Sn_6

curves below T_{CDW} has the distinct two-slope character [the blue 20 K curve in Fig. 5(c)]. This could be evidence of time-reversal symmetry breaking in the CDW state by weak magnetism or loop-current order. Reference [36] states that there is no evidence of static magnetic order but suggests that time-reversal symmetry might still be broken. Moreover, orbital current order has also been predicted to occur in ScV_6Sn_6 [69]. LuV_6Sn_6 does not have the CDW, and

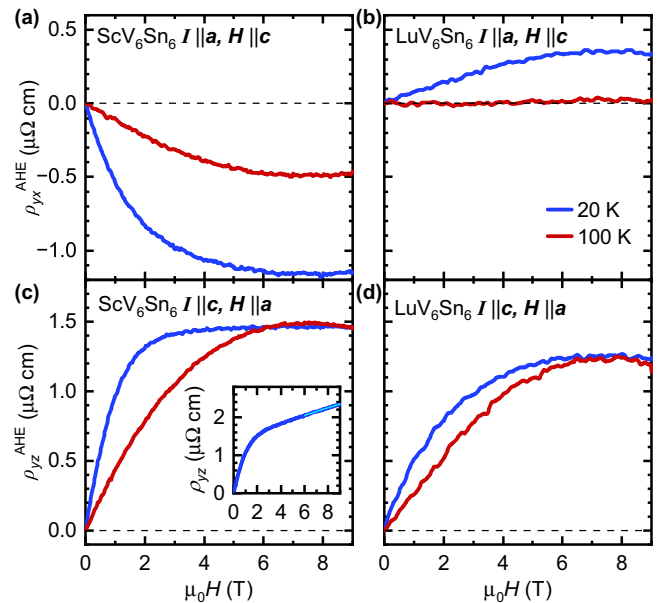


FIG. 5. Comparison of the extracted ρ_{yx}^{AHE} , (a) and (b), and ρ_{yz}^{AHE} , (c) and (d), taken by subtracting the local linear ordinary Hall background between 6 and 9 T in ScV_6Sn_6 and LuV_6Sn_6 . The inset in panel (c) illustrates the fitting (cyan line) done to estimate the normal Hall contribution.

its $\rho_{yz}^{\text{AHE}}(\mu_0 H)$ does not show this two-slope behavior. The different Hall behavior of the two compounds is emphasized by plotting the Hall conductivity σ_{ij} (Fig. S4 within the SM [38]). The AHE has also been reported in Ref. [70], but we provide a comparison to LuV_6Sn_6 . This comparison suggests that the AHE-like behavior in ScV_6Sn_6 arises from the CDW order.

IV. CONCLUSIONS

In summary, we have studied the anisotropic transport properties of two kagome compounds, ScV_6Sn_6 and LuV_6Sn_6 . While the compounds share similar band structures, the former exhibits a CDW phase at $T_{\text{CDW}} = 91$ K, and the latter does not. By comparing the properties of these materials, we uncover three key phenomena about ScV_6Sn_6 . First, ScV_6Sn_6 has strong magnetoresistance for current along the c axis that is absent in the Lu compound. This behavior occurs not only below T_{CDW} , but also extends to temperatures well above the transition suggesting a connection to CDW fluctuations. Second, we observe ScV_6Sn_6 has a sublinear temperature dependence of resistivity above T_{CDW} , which scales by $T^{\frac{3}{2}}$. This sublinear behavior also occurs in KV_3Sb_5 , RbV_3Sb_5 , and CsV_3Sb_5 suggesting this is a universal feature of the vanadium kagome CDW materials. Resistivity in the non-CDW compound LuV_6Sn_6 has a linear temperature dependence. Finally, we identify AHE-like behavior in ScV_6Sn_6 below T_{CDW} , which is absent in LuV_6Sn_6 . This could be evidence of time-reversal symmetry breaking or a consequence of reconstructing the intricate Fermi surface. Our comparison of magnetotransport in ScV_6Sn_6 and LuV_6Sn_6 reveals the unique influence of CDW order in the Sc material. These materials siblings will provide the foundation for understanding CDW order in the kagome metals.

ACKNOWLEDGMENTS

S.M., R.P.M., and D.G.M. acknowledge the support from AFOSR MURI (Novel Light-Matter Interactions in Topolog-

ically Non-Trivial Weyl Semimetal Structures and Systems), Grant No. FA9550-20-1-0322. S.M., W.R.M., and H.W.S.A. acknowledge the support from the Gordon and Betty Moore Foundation's EPiQS Initiative, Grant No. GBMF9069 to D.G.M. This publication is funded in part by a QuantEmX grant from ICAM and the Gordon and Betty Moore Foundation through Grant No. GBMF9616 to S.M. Y.Z. is supported by the National Science Foundation Materials Research Science and Engineering Center program through the University of Tennessee Knoxville Center for Advanced Materials and Manufacturing (DMR-2309083). Theory work at the Oak Ridge was supported by the U.S. Department of Energy (DOE), Office of Science, National Quantum Information Science Research Centers, Quantum Science Center (S.-H.K.), and by the U.S. Department of Energy, Office of Science, Office of Basic Energy Sciences, Materials Sciences and Engineering Division (J.W.V. and M.Y.). This research used resources of the Oak Ridge Leadership Computing Facility at the Oak Ridge National Laboratory, which is supported by the Office of Science of the U.S. Department of Energy under Contract No. DE-AC05-00OR22725 and resources of the National Energy Research Scientific Computing Center, a DOE Office of Science User Facility supported by the Office of Science of the U.S. Department of Energy under Contract No. DE-AC02-05CH11231 using NERSC Award No. BES-ERCAP0024568. L.L. acknowledges the support from the National Science Foundation under Award No. DMR-2317618 (transport properties) and the Department of Energy under Award No. DE-SC0020184 (magnetometry). We thank Brenden Ortiz and Andrea Capa Slinas for sharing the raw data for KV_3Sb_5 and CsV_3Sb_5 resistivity.

D.G.M. and S.M. conceived of the study. H.W.S.A., R.P.M., S.M., and W.R.M., grew the crystals. R.P.M., S.M., and W.R.M. performed the magnetotransport measurements and analyzed the obtained data. A.C., D.Z., G.Z., K.J., K.-W.C., L.L., N.P., and Y.Z. were involved in the discussion of the data. J.W.V., M.Y., S.-H.K., and Y.Z. performed the DFT calculations. S.M. wrote the manuscript with inputs from all the authors.

-
- [1] X. Teng, J. S. Oh, H. Tan, L. Chen, J. Huang, B. Gao, J.-X. Yin, J.-H. Chu, M. Hashimoto, D. Lu *et al.*, Magnetism and charge density wave order in kagome FeGe, *Nat. Phys.* **19**, 814 (2023).
- [2] A. O'Brien, F. Pollmann, and P. Fulde, Strongly correlated fermions on a kagome lattice, *Phys. Rev. B* **81**, 235115 (2010).
- [3] J. Wen, A. Rüegg, C.-C. J. Wang, and G. A. Fiete, Interaction-driven topological insulators on the kagome and the decorated honeycomb lattices, *Phys. Rev. B* **82**, 075125 (2010).
- [4] J.-X. Yin, B. Lian, and M. Z. Hasan, Topological kagome magnets and superconductors, *Nature (London)* **612**, 647 (2022).
- [5] L. Ye, S. Fang, M. G. Kang, J. Kaufmann, Y. Lee, J. Denlinger, C. Jozwiak, A. Bostwick, E. Rotenberg, E. Kaxiras, D. C. Bell, O. Janson, R. Comin, and J. G. Checkelsky, A flat band-induced correlated kagome metal, *Nat. Phys.* **20**, 610 (2024).
- [6] B. R. Ortiz, S. M. L. Teicher, Y. Hu, J. L. Zuo, P. M. Sarte, E. C. Schueller, A. M. M. Abeykoon, M. J. Krogstad, S. Rosenkranz, R. Osborn, R. Seshadri, L. Balents, J. He, and S. D. Wilson, CsV_3Sb_5 : A Z_2 topological kagome metal with a superconducting ground state, *Phys. Rev. Lett.* **125**, 247002 (2020).
- [7] B. R. Ortiz, P. M. Sarte, E. M. Kenney, M. J. Graf, S. M. L. Teicher, R. Seshadri, and S. D. Wilson, Superconductivity in the Z_2 kagome metal KV_3Sb_5 , *Phys. Rev. Mater.* **5**, 034801 (2021).
- [8] N. N. Wang, K. Y. Chen, Q. W. Yin, Y. N. N. Ma, B. Y. Pan, X. Yang, X. Y. Ji, S. L. Wu, P. F. Shan, S. X. Xu, Z. J. Tu, C. S. Gong, G. T. Liu, G. Li, Y. Uwatoko, X. L. Dong, H. C. Lei, J. P. Sun, and J.-G. Cheng, Competition between charge-density-wave and superconductivity in the kagome metal RbV_3Sb_5 , *Phys. Rev. Res.* **3**, 043018 (2021).
- [9] B. R. Ortiz, S. M. L. Teicher, L. Kautzsch, P. M. Sarte, N. Ratcliff, J. Harter, J. P. C. Ruff, R. Seshadri, and S. D. Wilson, Fermi surface mapping and the nature of charge-density-wave order in the kagome superconductor CsV_3Sb_5 , *Phys. Rev. X* **11**, 041030 (2021).

- [10] Z. Liu, N. Zhao, Q. Yin, C. Gong, Z. Tu, M. Li, W. Song, Z. Liu, D. Shen, Y. Huang, K. Liu, H. Lei, and S. Wang, Charge-density-wave-induced bands renormalization and energy gaps in a kagome superconductor RbV_3Sb_5 , *Phys. Rev. X* **11**, 041010 (2021).
- [11] K. Nakayama, Y. Li, T. Kato, M. Liu, Z. Wang, T. Takahashi, Y. Yao, and T. Sato, Carrier injection and manipulation of charge-density wave in kagome superconductor CsV_3Sb_5 , *Phys. Rev. X* **12**, 011001 (2022).
- [12] R. Tazai, Y. Yamakawa, S. Onari, and H. Kontani, Mechanism of exotic density-wave and beyond-migdal unconventional superconductivity in kagome metal AV_3Sb_5 ($A = \text{K}, \text{Rb}, \text{Cs}$), *Sci. Adv.* **8**, eabl4108 (2022).
- [13] H. Zhao, H. Li, B. R. Ortiz, S. M. L. Teicher, T. Park, M. Ye, Z. Wang, L. Balents, S. D. Wilson, and I. Zeljkovic, Cascade of correlated electron states in the kagome superconductor CsV_3Sb_5 , *Nature (London)* **599**, 216 (2021).
- [14] S.-Y. Yang, Y. Wang, B. R. Ortiz, D. Liu, J. Gayles, E. Derunova, R. Gonzalez-Hernandez, L. Šmejkal, Y. Chen, S. S. P. Parkin *et al.*, Giant, unconventional anomalous Hall effect in the metallic frustrated magnet candidate, KV_3Sb_5 , *Sci. Adv.* **6**, eabb6003 (2020).
- [15] F. H. Yu, T. Wu, Z. Y. Wang, B. Lei, W. Z. Zhuo, J. J. Ying, and X. H. Chen, Concurrence of anomalous Hall effect and charge density wave in a superconducting topological kagome metal, *Phys. Rev. B* **104**, L041103 (2021).
- [16] E. M. Kenney, B. R. Ortiz, C. Wang, S. D. Wilson, and M. J. Graf, Absence of local moments in the kagome metal KV_3Sb_5 as determined by muon spin spectroscopy, *J. Phys.: Condens. Matter* **33**, 235801 (2021).
- [17] H. W. S. Arachchige, W. R. Meier, M. Marshall, T. Matsuoka, R. Xue, M. A. McGuire, R. P. Hermann, H. Cao, and D. Mandrus, Charge density wave in kagome lattice intermetallic ScV_6Sn_6 , *Phys. Rev. Lett.* **129**, 216402 (2022).
- [18] N. J. Ghimire, R. L. Dally, L. Poudel, D. C. Jones, D. Michel, N. T. Magar, M. Bleuel, M. A. McGuire, J. S. Jiang, J. F. Mitchell, J. W. Lynn, and I. I. Mazin, Competing magnetic phases and fluctuation-driven scalar spin chirality in the kagome metal YMn_6Sn_6 , *Sci. Adv.* **6**, eabe2680 (2020).
- [19] R. P. Madhugaria, S. Mozaffari, H. Zhang, W. R. Meier, S.-H. Do, R. Xue, T. Matsuoka, and D. G. Mandrus, Topological nernst and topological thermal Hall effect in rare-earth kagome ScMn_6Sn_6 , *Phys. Rev. B* **108**, 125114 (2023).
- [20] G. Pokharel, S. M. L. Teicher, B. R. Ortiz, P. M. Sarte, G. Wu, S. Peng, J. He, R. Seshadri, and S. D. Wilson, Electronic properties of the topological kagome metals YV_6Sn_6 and GdV_6Sn_6 , *Phys. Rev. B* **104**, 235139 (2021).
- [21] H. Ishikawa, T. Yajima, M. Kawamura, H. Mitamura, and K. Kindo, GdV_6Sn_6 : A multi-carrier metal with non-magnetic $3d$ -electron kagome bands and $4f$ -electron magnetism, *J. Phys. Soc. Jpn.* **90**, 124704 (2021).
- [22] G. Pokharel, B. Ortiz, J. Chamorro, P. Sarte, L. Kautzsch, G. Wu, J. Ruff, and S. D. Wilson, Highly anisotropic magnetism in the vanadium-based kagome metal TbV_6Sn_6 , *Phys. Rev. Mater.* **6**, 104202 (2022).
- [23] E. Rosenberg, J. M. DeStefano, Y. Guo, J. S. Oh, M. Hashimoto, D. Lu, R. J. Birgeneau, Y. Lee, L. Ke, M. Yi, and J.-H. Chu, Uniaxial ferromagnetism in the kagome metal TbV_6Sn_6 , *Phys. Rev. B* **106**, 115139 (2022).
- [24] J. Lee and E. Mun, Anisotropic magnetic property of single crystals RV_6Sn_6 ($R = \text{Y}, \text{Gd-Tm}, \text{Lu}$), *Phys. Rev. Mater.* **6**, 083401 (2022).
- [25] Y. Hu, X. Wu, Y. Yang, S. Gao, N. C. Plumb, A. P. Schnyder, W. Xie, J. Ma, and M. Shi, Tunable topological Dirac surface states and van Hove singularities in kagome metal GdV_6Sn_6 , *Sci. Adv.* **8**, eadd2024 (2022).
- [26] Y. Gu, E. T. Ritz, W. R. Meier, A. Blockmon, K. Smith, R. P. Madhugaria, S. Mozaffari, D. Mandrus, T. Birol, and J. L. Musfeldt, Phonon mixing in the charge density wave state of ScV_6Sn_6 , *npj Quantum Mater.* **8**, 58 (2023).
- [27] W. R. Meier, R. P. Madhugaria, S. Mozaffari, M. Marshall, D. E. Graf, M. A. McGuire, H. W. S. Arachchige, C. L. Allen, J. Driver, H. Cao, and D. Mandrus, Tiny Sc allows the chains to rattle: Impact of Lu and Y doping on the charge-density wave in ScV_6Sn_6 , *J. Am. Chem. Soc.* **145**, 20943 (2023).
- [28] S. Cao, C. Xu, H. Fukui, T. Manjo, Y. Dong, M. Shi, Y. Liu, C. Cao, and Y. Song, Competing charge-density wave instabilities in the kagome metal ScV_6Sn_6 , *Nat. Commun.* **14**, 7671 (2023).
- [29] H. Tan and B. Yan, Abundant lattice instability in kagome metal ScV_6Sn_6 , *Phys. Rev. Lett.* **130**, 266402 (2023).
- [30] T. Hu, H. Pi, S. Xu, L. Yue, Q. Wu, Q. Liu, S. Zhang, R. Li, X. Zhou, J. Yuan, D. Wu, T. Dong, H. Weng, and N. Wang, Optical spectroscopy and band structure calculations of the structural phase transition in the vanadium-based kagome metal ScV_6Sn_6 , *Phys. Rev. B* **107**, 165119 (2023).
- [31] M. Tuniz, A. Consiglio, D. Puntel, C. Bigi, S. Enzner, G. Pokharel, P. Orgiani, W. Bronsch, F. Parmigiani, V. Polewczyk *et al.*, Dynamics and resilience of the charge density wave in a bilayer kagome metal, *Commun. Mater.* **4**, 103 (2023).
- [32] S. Cheng, Z. Ren, H. Li, J. S. Oh, H. Tan, G. Pokharel, J. M. DeStefano, E. Rosenberg, Y. Guo, Y. Zhang *et al.*, Nanoscale visualization and spectral fingerprints of the charge order in ScV_6Sn_6 distinct from other kagome metals, *npj Quantum Mater.* **9**, 14 (2024).
- [33] S.-H. Kang, H. Li, W. R. Meier, J. W. Villanova, S. Hus, H. Jeon, H. W. S. Arachchige, Q. Lu, Z. Gai, J. Denlinger *et al.*, Emergence of a new band and the Lifshitz transition in kagome metal ScV_6Sn_6 with charge density wave, [arXiv:2302.14041](https://arxiv.org/abs/2302.14041).
- [34] Y. Hu, J. Ma, Y. Li, D. J. Gawryluk, T. Hu, J. Teyssier, V. Multian, Z. Yin, Y. Jiang, S. Xu *et al.*, Phonon promoted charge density wave in topological kagome metal ScV_6Sn_6 , *Nat. Commun.* **15**, 1658 (2024).
- [35] S. Lee, C. Won, J. Kim, J. Yoo, S. Park, J. Denlinger, C. Jozwiak, A. Bostwick, E. Rotenberg, R. Comin *et al.*, Nature of charge density wave in kagome metal ScV_6Sn_6 , *npj Quantum Mater.* **9**, 15 (2024).
- [36] Z. Guguchia, D. J. Gawryluk, S. Shin, Z. Hao, C. Mielke III, D. Das, I. Plokhikh, L. Liborio, K. Shenton, Y. Hu *et al.*, Hidden magnetism uncovered in charge ordered bilayer kagome material ScV_6Sn_6 , *Nat. Commun.* **14**, 7796 (2023).
- [37] D. Di Sante, B. Kim, W. Hanke, T. Wehling, C. Franchini, R. Thomale, and G. Sangiovanni, Electronic correlations and universal long-range scaling in kagome metals, *Phys. Rev. Res.* **5**, L012008 (2023).
- [38] See Supplemental Material at <http://link.aps.org/supplemental/10.1103/PhysRevB.110.035135> for x-ray diffraction analysis, simulation of the Hall and magnetoresistivity, estimation of the

- activation energy of the insulating-like behavior of ρ_{zz} , change in the DOS across T_{CDW} , and Hall conductivity, which also includes Refs. [33,46,63,71].
- [39] P. Hohenberg and W. Kohn, Inhomogeneous electron gas, *Phys. Rev.* **136**, B864 (1964).
- [40] W. Kohn and L. J. Sham, Self-consistent equations including exchange and correlation effects, *Phys. Rev.* **140**, A1133 (1965).
- [41] G. Kresse and J. Hafner, *Ab initio* molecular dynamics for liquid metals, *Phys. Rev. B* **47**, 558 (1993).
- [42] P. E. Blöchl, Projector augmented-wave method, *Phys. Rev. B* **50**, 17953 (1994).
- [43] J. P. Perdew, K. Burke, and M. Ernzerhof, Generalized gradient approximation made simple, *Phys. Rev. Lett.* **77**, 3865 (1996).
- [44] Y. Zhang, Q. Xu, K. Koepnik, R. Rezaev, O. Janson, J. Železný, T. Jungwirth, C. Felser, J. van den Brink, and Y. Sun, Different types of spin currents in the comprehensive materials database of nonmagnetic spin Hall effect, *npj Comput. Mater.* **7**, 167 (2021).
- [45] K. Koepnik and H. Eschrig, Full-potential nonorthogonal local-orbital minimum-basis band-structure scheme, *Phys. Rev. B* **59**, 1743 (1999).
- [46] G. Zheng, Y. Zhu, S. Mozaffari, N. Mao, K.-W. Chen, K. Jenkins, D. Zhang, A. Chan, H. W. S. Arachchige, R. P. Madhugaria *et al.*, Quantum oscillations evidence for topological bands in kagome metal ScV_6Sn_6 , *J. Phys.: Condens. Matter* **36**, 215501 (2024).
- [47] R. D. Shannon, Revised effective ionic radii and systematic studies of interatomic distances in halides and chalcogenides, *Acta Cryst. Sec. A* **32**, 751 (1976).
- [48] L. Romaka, Y. Stadnyk, V. Romaka, P. Demchenko, M. Stadnyshyn, and M. Konyk, Peculiarities of component interaction in (Gd, Er)-V-Sn Ternary systems at 870 K and crystal structure of RV_6Sn_6 stannides, *J. Alloys Compd.* **509**, 8862 (2011).
- [49] C. Kittel and P. McEuen, *Introduction to Solid State Physics* (John Wiley & Sons, Hoboken, NJ, 2018).
- [50] N. W. Ashcroft and N. D. Mermin, *Solid State Physics* (Cengage Learning, Belmont, CA, 2022).
- [51] W. R. Meier, M.-H. Du, S. Okamoto, N. Mohanta, A. F. May, M. A. McGuire, C. A. Bridges, G. D. Samolyuk, and B. C. Sales, Flat bands in the CoSn-type compounds, *Phys. Rev. B* **102**, 075148 (2020).
- [52] C. Song, J. Park, J. Koo, K.-B. Lee, J. Y. Rhee, S. L. Bud'ko, P. C. Canfield, B. N. Harmon, and A. I. Goldman, Charge-density-wave orderings in LaAgSb_2 an x-ray scattering study, *Phys. Rev. B* **68**, 035113 (2003).
- [53] W. L. McMillan, Theory of discommensurations and the commensurate-incommensurate charge-density-wave phase transition, *Phys. Rev. B* **14**, 1496 (1976).
- [54] S. van Smaalen, M. Shaz, L. Palatinus, P. Daniels, F. Galli, G. J. Nieuwenhuys, and J. A. Mydosh, Multiple charge-density waves in $\text{R}_3\text{Ir}_4\text{Si}_{10}$ ($R = \text{Ho, Er, Tm, and Lu}$), *Phys. Rev. B* **69**, 014103 (2004).
- [55] A. Korshunov, H. Hu, D. Subires, Y. Jiang, D. Călugăru, X. Feng, A. Rajapitamahuni, C. Yi, S. Roychowdhury, M. G. Vergniory *et al.*, Softening of a flat phonon mode in the kagome ScV_6Sn_6 , *Nat. Commun.* **14**, 6646 (2023).
- [56] S. Li, B. Zeng, X. Wan, J. Tao, F. Han, H. Yang, Z. Wang, and H.-H. Wen, Anomalous properties in the normal and superconducting states of LaRu_3Si_2 , *Phys. Rev. B* **84**, 214527 (2011).
- [57] I. Y. Korenblit, A. Gerber, A. Milner, and M. Karpovsky, Sublinear temperature dependence of resistivity in metallic heterogeneous ferromagnets at high magnetic fields, *Phys. Rev. B* **59**, 131 (1999).
- [58] E. H. Hwang and S. Das Sarma, Linear-in- t resistivity in dilute metals: A fermi liquid perspective, *Phys. Rev. B* **99**, 085105 (2019).
- [59] Q. Yin, Z. Tu, C. Gong, Y. Fu, S. Yan, and H. Lei, Superconductivity and normal-state properties of kagome metal RbV_3Sb_5 single crystals, *Chin. Phys. Lett.* **38**, 037403 (2021).
- [60] R. Daou, N. Doiron-Leyraud, D. LeBoeuf, S. Y. Li, F. Laliberté, O. Cyr-Choinière, Y. J. Jo, L. Balicas, J.-Q. Yan, J.-S. Zhou *et al.*, Linear temperature dependence of resistivity and change in the Fermi surface at the pseudogap critical point of a high- T_c superconductor, *Nat. Phys.* **5**, 31 (2009).
- [61] A. Malinowski, M. F. Hundley, C. Capan, F. Ronning, R. Movshovich, N. O. Moreno, J. L. Sarrao, and J. D. Thompson, C-axis magnetotransport in CeCoIn_5 , *Phys. Rev. B* **72**, 184506 (2005).
- [62] N. Peshcherenko, N. Mao, C. Felser, and Y. Zhang, Sublinear transport in kagome metals: Interplay of Dirac cones and van Hove singularities, [arXiv:2404.11612](https://arxiv.org/abs/2404.11612).
- [63] S. Mozaffari, N. Aryal, R. Schönemann, K.-W. Chen, W. Zheng, G. T. McCandless, J. Y. Chan, E. Manousakis, and L. Balicas, Multiple Dirac nodes and symmetry protected Dirac nodal line in orthorhombic α - RhSi , *Phys. Rev. B* **102**, 115131 (2020).
- [64] C.-Z. Li, J.-G. Li, L.-X. Wang, L. Zhang, J.-M. Zhang, D. Yu, and Z.-M. Liao, Two-carrier transport induced Hall anomaly and large tunable magnetoresistance in Dirac semimetal Cd_3As_2 nanoplates, *ACS Nano* **10**, 6020 (2016).
- [65] L. Yu, C. Wang, Y. Zhang, M. Sander, S. Ni, Z. Lu, S. Ma, Z. Wang, Z. Zhao, H. Chen *et al.*, Evidence of a hidden flux phase in the topological kagome metal CsV_3Sb_5 , [arXiv:2107.10714](https://arxiv.org/abs/2107.10714).
- [66] C. Mielke, D. Das, J.-X. Yin, H. Liu, R. Gupta, Y.-X. Jiang, M. Medarde, X. Wu, H. C. Lei, J. Chang *et al.*, Time-reversal symmetry-breaking charge order in a kagome superconductor, *Nature (London)* **602**, 245 (2022).
- [67] Y. Hu, S. Yamane, G. Mattoni, K. Yada, K. Obata, Y. Li, Y. Yao, Z. Wang, J. Wang, C. Farhang *et al.*, Time-reversal symmetry breaking in charge density wave of CsV_3Sb_5 detected by polar Kerr effect, [arXiv:2208.08036](https://arxiv.org/abs/2208.08036).
- [68] D. R. Saykin, C. Farhang, E. D. Kountz, D. Chen, B. R. Ortiz, C. Shekhar, C. Felser, S. D. Wilson, R. Thomale, J. Xia, and A. Kapitulnik, High resolution polar Kerr effect studies of CsV_3Sb_5 : Tests for time-reversal symmetry breaking below the charge-order transition, *Phys. Rev. Lett.* **131**, 016901 (2023).
- [69] F. Grandi, A. Consiglio, M. A. Sentef, R. Thomale, and D. M. Kennes, Theory of nematic charge orders in kagome metals, *Phys. Rev. B* **107**, 155131 (2023).
- [70] C. Yi, X. Feng, N. Mao, P. Yanda, S. Roychowdhury, Y. Zhang, C. Felser, and C. Shekhar, Quantum oscillations revealing topological band in kagome metal ScV_6Sn_6 , *Phys. Rev. B* **109**, 035124 (2024).
- [71] J. Rodríguez-Carvajal, Recent advances in magnetic structure determination by neutron powder diffraction, *Phys. B: Condens. Matter* **192**, 55 (1993).